Renewable Energy 203 (2023) 131–141

Contents lists available at ScienceDirect

Renewable Energy

journal homepage: www.elsevier.com/locate/renene

A wind turbine blade leading edge rain erosion computational framework

Javier Contreras López [a,*], Athanasios Kolios [b], Lin Wang [c], Manuel Chiachio [d]

[a] Naval Architecture, Ocean and Marine Engineering, University of Strathclyde, 16 Richmond St, Glasgow G1 1XQ, Scotland, UK
[b] Department of Wind and Energy Systems Structural Integrity and Loads Assesment, Technical University of Denmark, Risø Campus Frederiksborgvej 399, Roskilde 4000, Denmark
[c] Department of Mechanical, Materials and Manufacturing Engineering, University of Nottingham, Nottingham NG7 2RD, UK
[d] Department of Structural Mechanics and Hydraulic Engineering, Andalusian Research Institute in Data Science and Computational Intelligence (DaSCI), University of Granada, Granada, 18071, Spain

ARTICLE INFO

Keywords:
Rain erosion
Wind turbine blade
Blade erosion degradation
Blade rain erosion
Energy production losses

ABSTRACT

Blades are one of the most important components, in terms of capital and operational costs, of wind turbines. The experienced acquired by the industry in the latest decades has shown that leading edge erosion is a problem of concern that impacts the reliability of the blade and the power production of the turbine, among others. This study provides a framework to estimate leading edge erosion evolution and energy production degradation throughout time to apply in operation and maintenance decision making. It is based on the generation of synthetic wind and rain data based on observations from the site and ERA5 reanalysis data, whirling arm test data of erosion protection coatings, along with aerodynamic polar curves for clean and eroded airfoils of the blade. Rain erosion is calculated based on impingement, and assumed to be linearly accumulated using the Palmgren–Miner rule. Synthetic wind and rain time series are used to evaluate 25-year erosion degradation and energy production scenarios. A case study using the 5MW NREL's wind turbine located in the North Sea has been analysed with the proposed framework showing maximum annual energy production losses in the range of 1.6–1.75% and first erosion failure between years 2 and 6.

1. Introduction

The high costs of offshore wind turbine operation and maintenance (O&M) and the difficulty to perform maintenance on their parts due to weather and time constraints, pose a significant importance in risk identification and maintenance planning. The blades have been highlighted as one of the parts with the highest risk of failure within the turbine [1]. Among the critical subcomponents of the blade, the leading edge is one of the most relevant due to the high velocities experienced by the sections close to the tip, as depicted in Fig. 1. Blade leading edge erosion is a phenomenon that is produced due to many factors: environmental degradation due to temperature, moisture, UV radiation and fatigue degradation of the edge protective coating due to rain, and hail or wind-borne debris impacting the blade during its rotation, to cite but the most important. Additionally, its initiation may be favoured by manufacturing defects in the application of the leading edge protection systems or impacts during the handling of the blade in the transport and construction phase. The erosion produces the detachment of fragments of the coating from the blade and also modify the airfoil geometry, which alter the performance of the blade in many aspects: aerodynamically, acoustically, and if left unattended, structurally.

The effects of this erosion progress from turbine power degradation to potential damage to the skin laminates of the shell, evolving into more severe damage types such as delamination and the failure of the joint between shells. The power degradation of the blade is just a result of the modification of the aerodynamic properties of the affected sections, which produce a reduction of lift and an increase in drag [2]. This power degradation occasions annual energy production (AEP) losses, the range of which is not yet clear due to the high uncertainty in the degradation process, the coating material characteristics, and the airfoil aerodynamic performance, among others.

In the literature, there are several studies focusing on the leading edge erosion problem of wind turbine blades, and the reader is referred to [4,5] for a comprehensive overview of methods.

In terms of airfoil aerodynamic performance, Gaudern et al. [2] studied the lift and drag variation of different airfoils at different erosion stages using wind tunnel tests. Their results showed a lift reduction about 3%–10% for both airfoils, which increased with the erosion progression. In a similar manner, Sareen et al. [6] carried out a comprehensive wind tunnel test study for the DU 96-W-180 airfoil for different erosion levels with lift reductions in the range of 5%–15%

* Corresponding author.
E-mail address: javier.contreras-lopez@strath.ac.uk (J. Contreras López).

https://doi.org/10.1016/j.renene.2022.12.050
Received 21 April 2022; Received in revised form 10 October 2022; Accepted 13 December 2022
Available online 14 December 2022

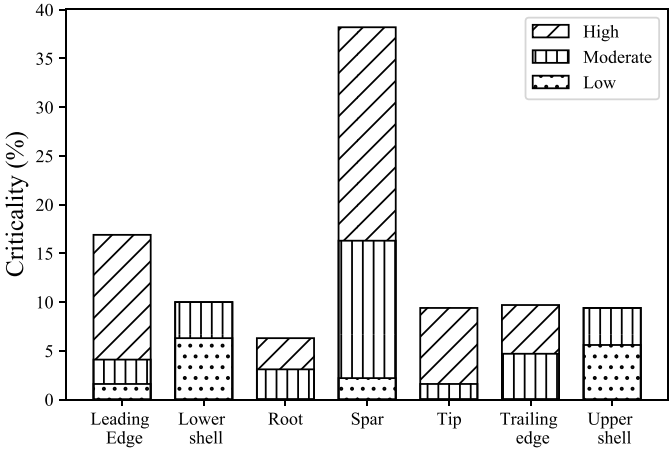

Fig. 1. Criticality by blade component.
Source: [3].

and an AEP loss between 3 and 23%. Schramm et al. [7] opted for a numerical approach using 2D computational fluid dynamics (CFD) to determine the behaviour of wind turbines with eroded blades. Airfoil polars were generated using CFD which were further employed to obtain wind turbine loads and power curves by the blade element momentum (BEM) theory. The referred study reported AEP losses of about 8%.

In a first effort to better understand the relation between erosion models and their mechanical effects on the turbines blades, Eisenberg et al. [8] made use of the rain erosion computational model developed by Springer [9] along with proprietary wind turbine historical observations to calibrate a model able to estimate rain mechanical erosion. Besides, a BEM code was applied, along with eroded aerodynamic data from [6] to evaluate AEP losses with results around a 1.7% for turbines with a 50% time spent operating at rated power. More recently, [10] provided experimental and numerical CFD studies to evaluate the effects of the erosion degradation of airfoils. Similarly, Cappugi et al. [11] used an approach based on artificial neural networks (ANNs) using wind turbine and eroded blade data, along with CFD and BEM theory to provide power curves, loads, and AEP of turbines with eroded blades at different erosion levels. AEP losses between 2.2 and 4% were reported for advanced erosion states. An uncertainty quantification on the effects of rain-induced erosion on AEP was performed by Papi et al. [12], where average AEP losses of up to a 1.5% were estimated.

Regarding active erosion protection systems, there are some works covered in the literature, like the one by Hasager et al. [13] who performed a lifetime assessment of leading edge protections for turbines in Danish Seas considering a Vestas V52 turbine using the kinetic energy and accumulated rain damage models. Their results show expected leading edge protection lifetimes between 2 and 13 years. Also, Bech et al. [14] studied the use of smart turbine control to reduce the rotation speed of the blades and diminish the effect of rain erosion in a Vestas V52 850 kW wind turbine. In a different study, Hasager et al. [15] studied the expected AEP loss and leading edge lifetime of a number of sites in the North and Baltic sea. Lifetimes between less than 1 year and more than 25 were reported and a potential O&M cost reduction using an active erosion safe operation mode of around 70% compared to the normal operation of the turbine.

According to the authors' opinion, despite the efforts recently made to model the erosion influence on the aerodynamics and mechanical behaviour of a turbine blade (including its effects on AEP), the inherent uncertainty around this damage mode has not been considered in a proper manner. The lack of knowledge about the expected life of erosion protection coatings for particular site conditions implies a barrier for the application of such preventive methods. Moreover, the current state of the knowledge in the open literature calls for a framework to determine AEP loss with less uncertainty and to evaluate the need of corrections, if required, in terms of operation and/or maintenance for wind farm operators. This manuscript provides an efficient framework to estimate the evolution of erosion degradation based on rain erosion test data considering weather uncertainty. Furthermore, it provides an estimate of the power losses occasioned by it and an estimation of the remaining useful life of the blade. The proposed framework can be employed to investigate the O&M costs of different leading edge protection solutions in the design stage for a particular site and for the latter O&M planning of an operative turbine with potential benefits in cost reductions in both stages.

The paper is structured as follows: Section 2 provides some fundamentals about the process of leading edge erosion, its causes and effects, the typical erosion protection configurations found in wind turbine blades, and current testing procedures. Section 3 describes the proposed modelling framework for AEP degradation calculation. In Section 4, a case study for a 5 MW NREL bottom-fixed offshore wind turbine using the proposed framework is presented. Finally, conclusions derived from the use of this framework are drawn in Section 5.

2. Fundamentals about leading edge erosion

Leading edge blade erosion is a phenomenon that has attracted the attention of both the research community and the industry during the latest decades [6,8,16–19]. This attention has been accentuated by the increase in rotor diameter and power of the turbines. The elevated speeds experienced by the sections closer to the tip of the blade increase the impact energy of rain, hail, insects and other wind-borne particles. Most of the experimental studies have been focused on the damage occasioned by rain, but numerical studies considering the impact of general wind-borne particles can also be found in the literature [20,21]. Rain-related erosion is thought to be more predominant in offshore wind farms, and so the effort has been more focused on this aspect.

In the case of rain erosion, most leading edge failures are believed to be developed due to fatigue of the coatings that take place due to accumulated impacts of rain droplets. The transient stress waves that are occasioned in the surroundings of the location of the droplet's impact accumulate fatigue cycles in the coating layers that, after some time, result in the loss of coating mass [22]. The rate of progression of this phenomenon is influenced by different factors: material properties, meteorological and wind turbine operating characteristics are among the ones highlighted as the most influential [8].

With regard to the materials used to protect against this phenomenon, a variety of leading edge protection configurations can be found in the literature [23–27]. Leading edge protection coatings can be applied through in-mould manufacturing during the manufacturing of the shells of the blade or a post-mould application in the leading edge erosion-prone areas of the blade. The configuration of the coating protection adopts different schemes, with the most basic consisting of 2–3 layers of protective coating over a layer of filler, to more advanced configurations including a layer of primer between the coating and the filler. The usual configurations of the protection system are shown in Fig. 2.

The evolution of impingement erosion has been discretised in different stages in the literature [6,8,28]. The first stage, known as the incubation period (Stage 0), where the fatigue limit of the coating has not been consumed, is characterised by no external signs of degradation or mass loss of the coating. After this, minor pits are formed in the LEP (leading edge protection) coating, with an increase in rugosity (Stage 1). This is followed by an increased mass loss stage, where minor flakes of the topcoat are removed and the filler can be intermittently seen below the topcoat (Stage 2). Then, the erosion progresses until the epoxy below the filler can be intermittently seen whilst the filler is not completely removed (Stage 3). The filler is then completely removed

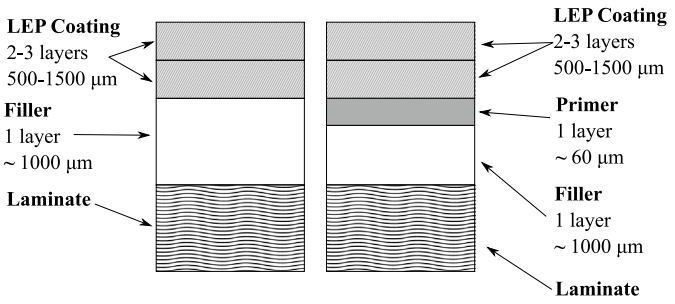

Fig. 2. Typical leading edge protection configurations.
Source: Adapted from [26].

leaving the epoxy exposed, thus being this the final erosion stage of the coating, but having the risk of progressing to the laminate layers of the shell and creating delaminations and loss of mass of the sandwich panel (Stage 4). The effects of erosion have different implications through its progression and can affect the aerodynamic, acoustic, and structural behaviour of the blade.

Concerning the acoustic effects of the leading edge erosion, the emissions can be increased up to a 10% [29], which, in some cases, could be important for the negative environmental impact that this could produce. Also, the aerodynamic effects affect directly the power output of the turbine, producing a loss of power at below-rated wind speeds. This means that not only the turbine characteristics but also the rain and wind characteristics of the site have an impact on the energy production losses of the blade.

Finally, the structural integrity of the blade is also compromised. The risk of cracks, fatigue damage and delamination grows as the erosion progresses through the protection layers and less impact energy is absorbed by them, until the laminate is exposed and the risk of structural damage is high. During the incubation period, there are no effects on the structural integrity of the blade, and only minimal to negligible effects can be observed on its aerodynamic performance. When the filler is exposed, the aerodynamic effects start growing in importance while the structural damage is still minor. Finally, when the epoxy is exposed, the structural integrity decays until maintenance of the leading edge is required to recover the integrity of the blade. Some guidance can be found in the literature published by Bladena [28] for the O&M actions related to leading edge erosion. The recommendation given in the referred work is to perform repairs within 6 months if the erosion reaches the laminate, and within 3 months if it reaches the second layer of the laminate to avoid compromising the structural integrity of the whole blade.

Rain erosion testing has been performed for several applications such as steam and gas turbines, cooling pipes of nuclear power plants, fan blades of aero engines, and wind turbines, with different impact speeds and droplet diameters. A summary of the different existing testing systems can be found in [30,31]. To evaluate the performance of erosion protection systems for wind turbine blades, the most common experimental testing arrangements are the stationary sample jet impacted by an interrupted jet or water jet slugs and the whirling arm testers [32]. While the stationary jet is a more simple arrangement and facilitates the sampling methods, using impact velocities higher than the terminal speed breaks the drops. Whirling arm testers produce the impact velocity by rotating the sample instead of accelerating the water droplet, which reduces the difficulties in producing high impact velocities but increases the difficulty in the sampling process. These tests aim to generate Wöhler-like curves with the impact speed versus the accumulated impacted water, time to failure, or specific impacts. In this study, data from whirling arm tests available in the literature will be used to evaluate the effects of erosion degradation. Notwithstanding, these tests are argued to not reproduce the diversity of conditions experienced in the operation of turbine blades, which include intermittent

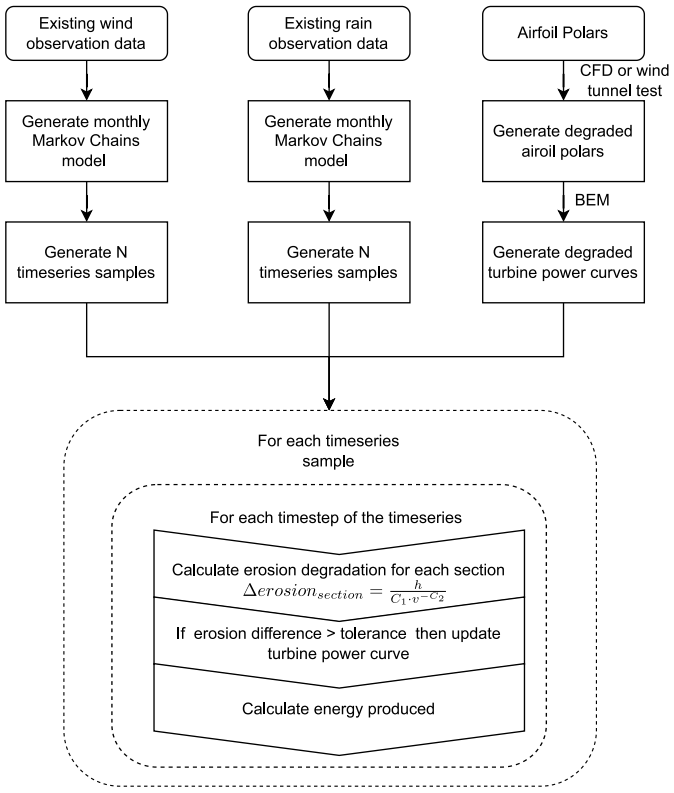

Fig. 3. Computation framework.

rain, distributed raindrop sizes, and varying impact energy and droplet sizes. Some current research focused on these aspects are the studies of Bech et al. [33], who performed experimental tests to study the effect of drop size in rain erosion tests and lifetime prediction, or Verma et al. [34] who developed a probabilistic rainfall model to estimate the leading edge lifetime of coating systems in which the effects of rain intensity and droplet size are analysed. While rain erosion tests have been useful to comparatively analyse the performance of different protection systems, their application to lifetime analysis seems to be not so accurate for some researchers [8,35].

3. Proposed modelling framework

The proposed framework is depicted in Fig. 3. It starts with the generation of random rain and wind time series, which can be based on weather observations or ERA5 reanalysis data from the location of the turbine [36]. Additionally, aerodynamic performance polar curves of eroded airfoils are obtained. Alternatively, a full 3D CFD simulation of the blade can be performed. Notwithstanding, due to the computational cost of each simulations and the number of simulations needed to capture different states of degradation of the blade, the 2D approach was preferred. Also, the use of the BEM theory allows the integration of polar curves obtained numerically or experimentally in a more practical and efficient way. Fig. 3 also indicates that using the modified polar curves, the operating power curves of different eroded states of the blades are calculated. Once this information is available, the synthetic weather data and the estimated aerodynamic performance of the airfoils are combined to calculate erosion and energy production at each timestep using the appropriate power curve representing the degraded state of the blade under the BEM theory.

3.1. Weather time series generation

Weather time series with high granularity and quality are typically difficult to obtain for a particular wind turbine location. A feasible

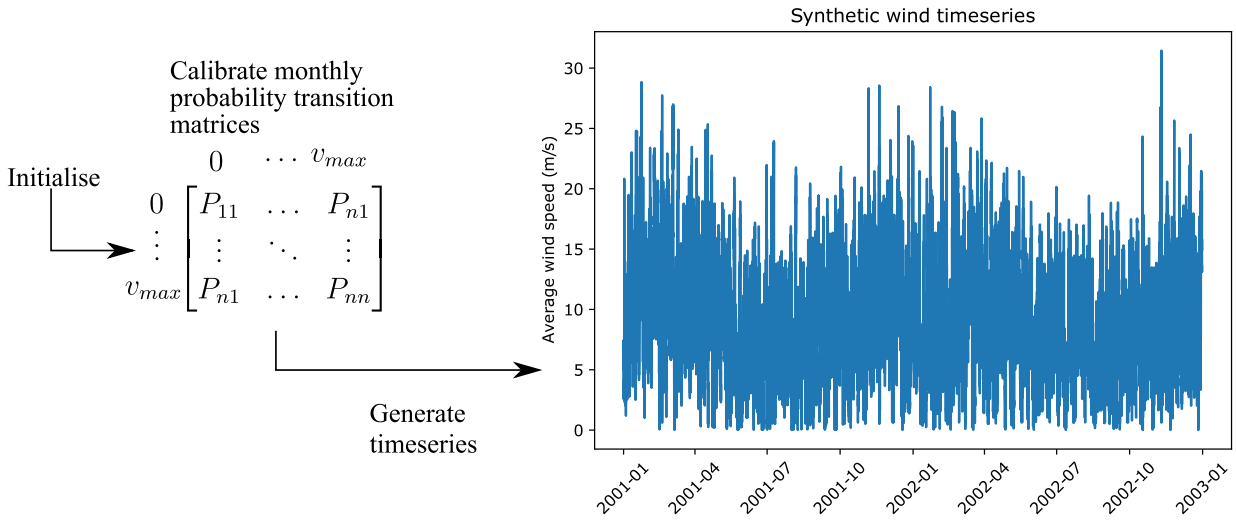

Fig. 4. Synthetic wind data generation process. Subindex n refers to the number of bins in which wind speed is discretised.

alternative to obtain such weather data, which ranges between 20 and 25 years long, is the use of Markov chains [37] models to synthetically generate datasets while preserving the weather characteristics of the site. Therefore, random rain and wind scenarios can be generated to account for a probabilistic analysis of the erosion degradation of the blade. In this work, 10-minute average data for wind and rain are used. Wind and rain have been modelled as statistically independent variables. For wind data, a Markov probability transition matrix with 0.5 m/s bins has been calibrated using FINO1 [38] wind observation data. To avoid problems with the seasonality behaviour of wind, a different probability transition matrix per month was considered, along with a general annual wind transition probability matrix, to avoid the wind speed falling in a range where there are no occurrences in a month. For clarity, the process is schematically illustrated in Fig. 4. For the rain data, the shorter available data range called for the use of a different approach based on modelling rain intensity through monthly Weibull probability density functions, whereby Markov probability transition matrices with rain/no rain probability were obtained. While this approach results in unrealistic variability of rain intensities, it is assumed to not have a significant influence on the results of this study. The process is illustrated in Fig. 5.

3.2. Airfoil performance estimation

CFD simulations are used for the estimation of the polar curves of the degraded airfoils. The Navier–Stokes CFD code from ANSYS FLUENT® is used in this work. The air flow has been modelled as incompressible and single-phase fluid. The pressure-based steady Reynolds-averaged Navier–Stokes (RANS) equations are solved in all cases, and the turbulence closure is accomplished utilising the Menter's two-equation $k-\omega$ shear stress transport (SST) model [39]. Polar curves are obtained at Reynolds numbers in the range $1 \cdot 10^6$ to $9 \cdot 10^6$ every $1 \cdot 10^6$ and in a range of angles of attack from $-20°$ to $20°$ every $1°$. The degradation of the leading edge was modelled by adjusting the equivalent sand grain roughness height as proposed in [40] based on the stage 4 erosion parameters defined in [6]. The equivalent sand grain roughness height, k_s, was set to a value of $k_s/c = 0.0076$ for the final degraded state, where c is the chord of the airfoil. The roughness modification is applied in a length of a 10% of the chord in the top shell and a 13% in the bottom shell, to account for the blade increased erosion of the bottom shell during the pitching of the blade.

Finally, the resulting CFD-generated lift and drag curves were corrected for 3D stall effects and extrapolated for the whole $-180°$ to $+180°$ using the Viterna method [41] for their use in the BEM code OpenFAST [42].

3.3. Erosion degradation model

As previously mentioned in Section 1, there are different models to account for the erosion progression in the blades, where the most recent are based on a droplet impact model to establish stress states that consume the fatigue life of the coating. In most of the studies encountered in the literature, the analytical description of this phenomenon follows the model developed by George Springer [9], where the erosion resistance is fitted to a curve based either on impact energy damage, specific impacts, accumulated rain under the rotor or impingement. Thus, the impingement model will be used here. The rain impingement, referred to here as h, can be calculated as follows:

$$h = \psi \cdot t \cdot v(r) \tag{1}$$

where t is the time, $v(r)$ the local rotor speed, and ψ, the volume concentration of rain in the air, which can be calculated as shown below:

$$\psi = I / v_{drop} \tag{2}$$

being I the rain intensity, and v_{drop} the droplet velocity at the rotor plane. The term v_{drop} can be obtained as the terminal velocity using the empirical relationship found in [9] and the droplet size being the median for the rain intensity distribution proposed in [43]. Experimental test data from whirling arm tests [32] is used to determine the number of impacts or accumulated energy of impact required to produce erosion in the material. These tests are performed at different speeds to provide a fit for the number of impacts causing fatigue damage. The fitting curve equation is described as follows:

$$H = C_1 \cdot v(r)^{-C_2} \tag{3}$$

where H is the accumulated rain impingement to erosion failure at local rotor velocity, and C_1, C_2 are material parameters calibrated using experimental test data. To evaluate the damage progression, linear damage accumulation using the Palmgren–Miner damage rule is assumed, as typically done to simplify damage accumulation for different amplitude fatigue damage [44]. Therefore, the erosion life consumption at timestep i, namely ΔD_i, will be computed as:

$$\Delta D_i = \frac{h_i}{C_1 \cdot v(r)_i^{-C_2}} \tag{4}$$

where h_i is the accumulated rain impingement, and $v(r)_i$ the local rotor speed at timestep i.

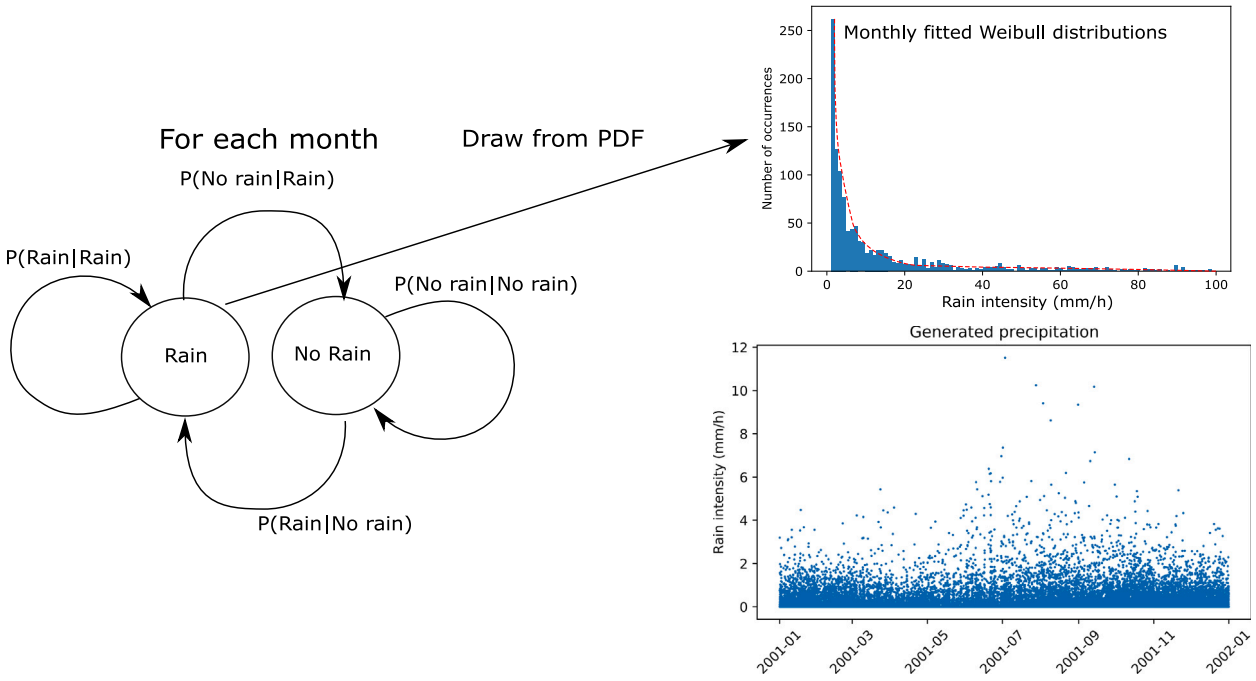

Fig. 5. Synthetic wind data generation process.

Table 1
5 MW NREL Turbine data.
Source: Data extracted from [45].

Property	Value
Rated power	5 MW
Control	Variable speed, collective pitch
Drivetrain	High speed, multiple-stage gearbox
Rotor diameter	126 m
Hub height	90 m
Cut-In/Rated/Cut-out wind speed	3 m/s/11.4 m/s/25 m/s
Cut-in/Rated rotor speed	6.9 rpm, 12.1 rpm
Rated tip speed	80 m/s

Table 2
5 MW NREL Blade Airfoil data.
Source: Data extracted from [45].

Station id	*R* (m)	*Twist* (°)	*Chord* (m)	*Airfoil*
1	2.87	13.31	3.542	Cylinder
2	5.6	13.31	3.854	Cylinder
3	8.333	13.31	4.167	Cylinder
4	11.75	13.31	4.557	DU40 A17
5	15.85	11.48	4.652	DU35 A17
6	19.95	10.16	4.458	DU35 A17
7	24.05	9.1	4.249	DU30 A17
8	28.15	7.79	4.007	DU25 A17
9	32.25	6.54	3.748	DU25 A17
10	36.35	5.36	3.502	DU21 A17
11	40.45	4.18	3.256	DU21 A17
12	44.55	3.13	3.010	NACA64 A17
13	48.65	2.32	2.764	NACA64 A17
14	52.75	1.53	2.518	NACA64 A17
15	56.17	0.86	2.313	NACA64 A17
16	58.9	0.37	2.086	NACA64 A17
17	61.63	0.11	1.419	NACA64 A17

3.4. Calculation of degraded power curves

The calculation of the power curves has been performed with the BEM method using OpenFAST, running 200 second simulations of uniform wind fields at fixed intervals of wind speeds of 1 m/s from the cut-in to the cut-out wind turbine wind speeds. Airfoil sections are defined at the desired points of the blade at which the erosion is computed, whereas for the remaining control points, airfoil characteristics are averaged from the two closest stations. Note that enough simulation time is required to provide steady-state responses of the system and also to avoid transient disruptions of the results. These curves have been used to compute 10-min average energy production at each simulation timestep.

3.5. Erosion progression estimation

The estimation of erosion degradation has been computed according to a rain impingement accumulation fitted curve, as proposed in [13]. An incubation period of 30% of the total life has been assumed for the leading edge erosion protection system and, from that standpoint, linear degradation is assumed until the final erosion stage. Aerodynamic properties were obtained using CFD simulations with modifications of leading edge roughness and corrected for 3D stall, which could be substituted by wind tunnel test data, if available. For the 25-year meteorological time series required (precipitation and wind), observations from meteorological stations are required, otherwise ERA5 [36] data can be used to produce synthetic time series using Markov Chains with monthly fitted transition matrices. Leading edge erosion degradation shall be computed for, at least, the last third of the blade along with the time series. In this case, 10-min average wind speed and rain intensity data were used. The variability produced by using lower resolution data (i.e. 1-h average data or 30-min average data) has not been studied here, and it is left as one of the desirable further works of this research. Eroded airfoil polar curves have been discretised in segments of 10% so that the 10% degraded curve is used for degradation ranges between 5% and 15%, the 20% for the range 15% to 25% and so on until the final degradation of the section.

4. Case study

To exemplify the use of the proposed framework, a case study is presented and analysed in the sections below.

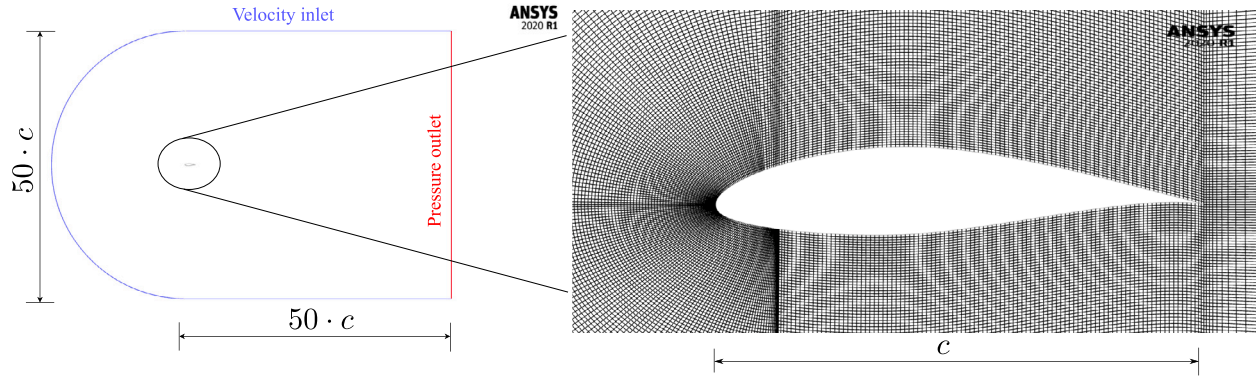

Fig. 6. CFD setup.

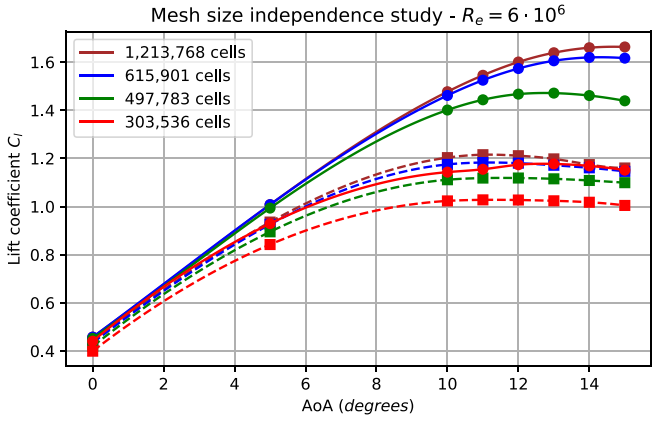

(a) Mesh size independence study (continuous and dashed lines represent the clean and eroded case respectively).

Cells	$C_{l,max}$(clean)	$C_{l,max}$(eroded)
1,213,768	1.6632	1.2154
615,901	1.6197	1.1828
497,783	1.4714	1.1186
303,536	1.1771	1.0278

(b) Mesh independence results.

Fig. 7. Mesh independence study results.

4.1. Turbine and blade data

For this study, the 5 MW NREL wind turbine [45] has been chosen. The main characteristics of the turbine are shown in Table 1, where the airfoils used in the blade are shown in Table 2. In this case, only the erosion effect on the NACA64 airfoil was investigated due to the lower velocities experienced by the remaining airfoils of the blade. Leading edge erosion damage is more prone to appear on the outermost part of the blade due to the higher impact energy of the rain in those areas.

4.2. CFD setup

C-shaped structured mesh has been used for this analysis. Its structure and the boundary conditions used in the simulations are shown in Fig. 6. To provide meaningful results, a mesh size independence study and a validation with published NACA64 A17 results has been performed, as is shown next.

4.2.1. Mesh size independence analysis

In this work, four different mesh sizes were explored, with a number of cells ranging from $3{\cdot}10^5$ to more than $1.2 \cdot 10^6$ for different angles of attack and Reynolds number of $6 \cdot 10^6$. The CFD simulation was solved utilising the Menter's two-equation $k-\omega$ shear stress transport (SST) model. The results, which are shown in Fig. 7, show a close agreement of the lift coefficients for the two finer meshes ($1.2 \cdot 10^6$ and 615,00 cells, respectively) with maximum lift coefficient values as shown in the table of Fig. 7. Considering the results presented and to reduce the computational effort of this case study, the second finer mesh (615,901 cells) was selected.

4.2.2. Study of the influence of y^+

For the sake of efficiency, the effect of wall functions was investigated and solutions were compared for the cases of average y^+ values of approximately 1 and 87. The model with the greater value of y^+ makes use of wall functions to solve the flow within the boundary layer. The distribution of y^+ values along the chord is shown in Fig. 8. Fig. 9 shows the results of lift coefficient for different angles of attack and a $R_e = 6 \cdot 10^6$ for the studied models. The results show a good agreement for the lift of the airfoil in the linear and non-linear parts of the graph, with a slight overestimation of lift by the model using a $y^+ \sim 87$. Considering the efficiency of both models, the model with the $y^+ \sim 87$ was chosen in this case.

4.2.3. Validation

To evaluate the accuracy of our CFD setup, simulation results were compared with NACA64 experimental aerodynamic coefficient results from [46] in Fig. 10. Note that, in general, the simulation results show a good agreement in terms of the overall behaviour of the flow detachment around 12°–14°, and generally a fair agreement in terms of maximum lift coefficient. Note also that the lift values of the simulations are in close agreement with the experimental results for the range −5° to 5° of angle of attack (AoA), while the model tends to overestimate them for higher AoAs.

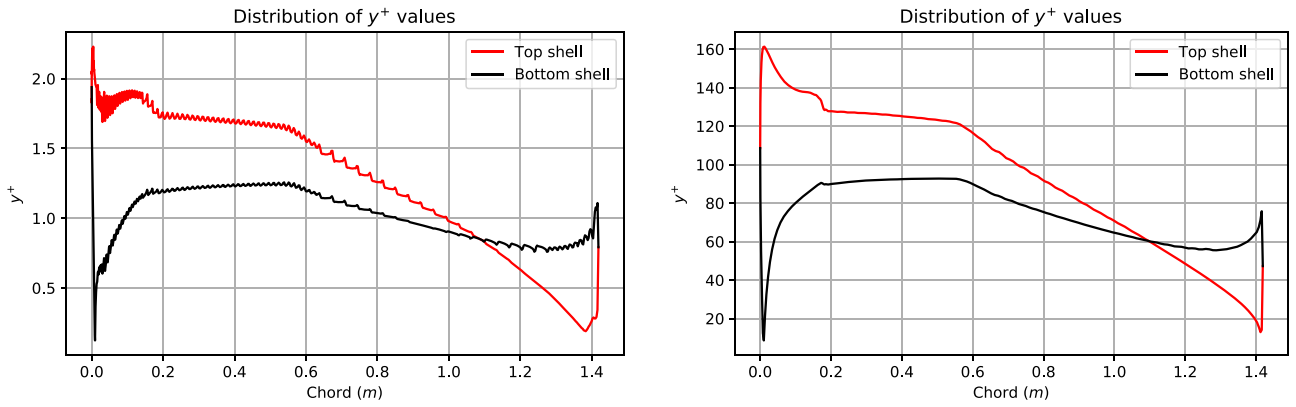

(a) Low y^+ mesh. (b) Large y^+ mesh (wall functions).

Fig. 8. Distribution of y^+ value for the studied meshes.

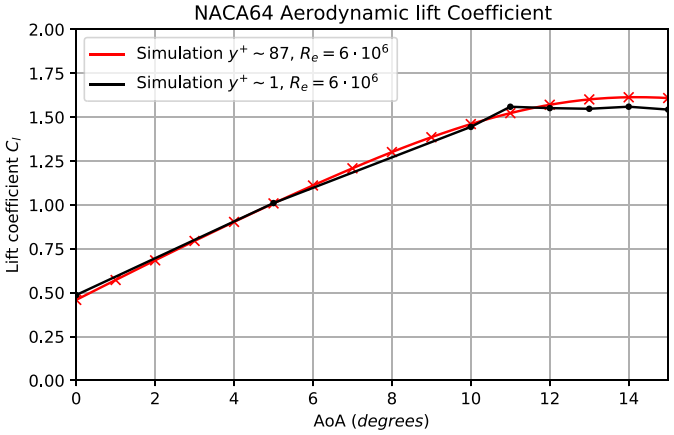

Fig. 9. Lift results using different y^+ values.

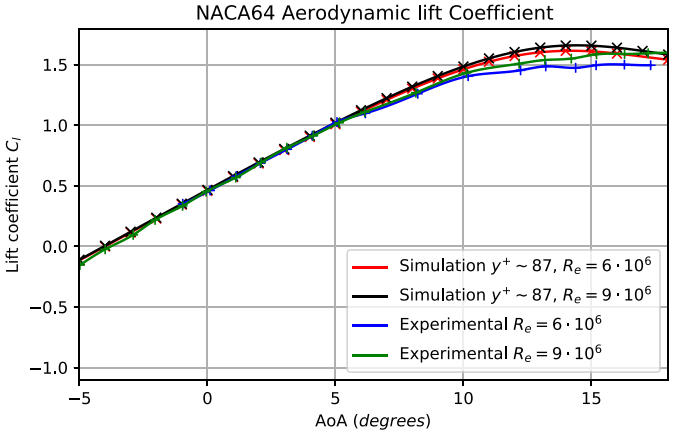

Fig. 10. NACA64 CFD setup validation with experimental results from [46].

Baseline and eroded aerodynamic properties of the NACA64 airfoil were generated using Fluent Ansys following the procedure detailed in Section 3.2 and the CFD setup explained above. The resulting lift coefficients for the baseline and eroded profiles after their correction for 3D stall effects and extrapolation for the whole −180° to +180° range by the Viterna method, are shown in Fig. 11.

Moreover, Fig. 12 shows a comparison between the baseline power curve of the wind turbine and a power curve considering the full

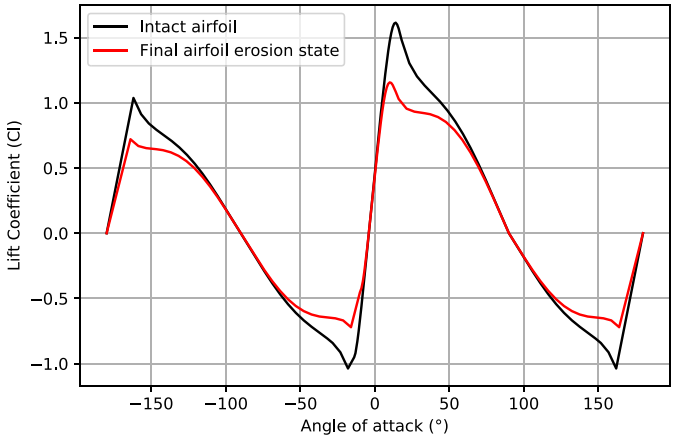

Fig. 11. NACA64 CFD results extrapolated Polars $Re = 9 \cdot 10^6$ after 3D stall correction and extrapolation.

degradation of sections 12 to 17 (from 45 to 62.5 m from the root of the blade), which would simulate the final erosion state of the blade.

4.3. Weather data

In this work, the location of the turbine is assumed in the vicinity of FINO1 offshore measurement platform, sited 45 km north of the coast of the island of Borkum, Germany. Wind speed data was obtained from the FINO1 database and rain data from ERA5 reanalysis and used to calibrate the Markov Chains models as explained in Section 3.1. A hundred random 25-year wind and rain time series were generated. The average values of 10-min wind speed and rain intensity by month are shown in Figs. 13 and 14.

For the case of wind, the generation of time series follows the overall monthly shape with a lag, producing a slight underestimate of the average wind speed (Fig. 13(a)). The annual wind speed distribution of the observed and synthetically generated data are presented in Fig. 13(b). It can be seen that the distribution of the generated data is slightly shifted towards lower wind speeds; however, the overall shape is maintained. Separately, the synthetic rain generation time series process seems to provide a closer match with the average weather observations, even though there is also a slight underestimation of the average rain intensity for some months.

4.4. Erosion leading edge protection configuration

Here, several erosion protection configurations are investigated. The different configurations are labelled as '*3Layer*', '*GS*', '*GC*', and '*GA*'.

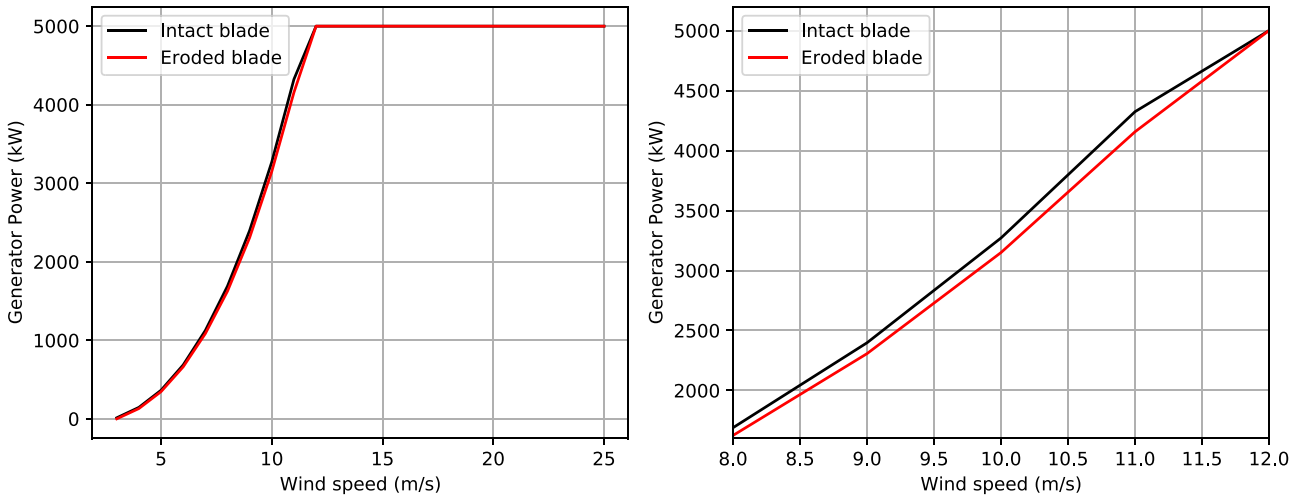

Fig. 12. Turbine original vs. degraded power curve. In the rightmost panel, the plot is zoomed in for the range 8 to 12 m/s of wind speed.

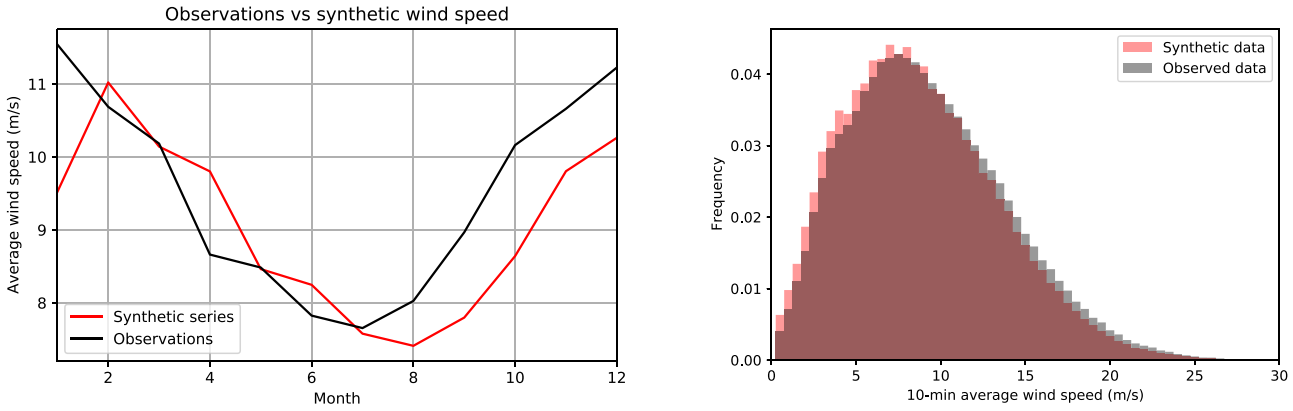

(a) Average monthly wind speed - Observed vs Synthetic data.

(b) Wind speed distribution - Observed vs Synthetic data.

Fig. 13. Weather data used in the case study.

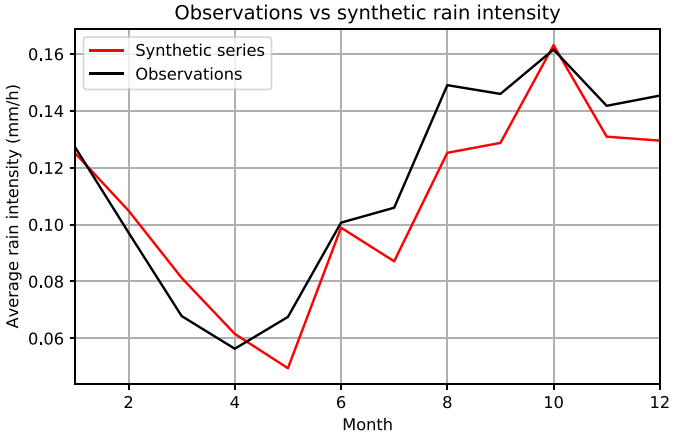

Fig. 14. Average rain intensity - Observed vs. Synthetic data.

The '*GC*' and '*GA*' configurations are simpler, consisting only of a single layer of PU elastomeric coating, while '*3Layer*' and '*GS*' are more complex consisting of several coating layers and a filler. Their characteristic whirling arm test SN curves are shown in Fig. 15.

It is important to note that these curves represent the average behaviour of a number of tests, and that the variability shown by the different samples can represent a significant impact on the final service life of the erosion protection coating. This issue can be overcome with the use of inspection data, with which the model can be corrected and the behaviour of the actual erosion protection coating of the blade captured for better O&M optimisation.

4.5. Erosion degradation

The results of the progression of erosion degradation is shown in Fig. 16. This figure represents the time at which the total degradation is reached for the sections at which the erosion degradation has been calculated. The results show that the leading edge coatings composed of 1–2 layers (namely, *GC* and *GA*) have a faster progression of the erosion front, reaching the erosion failure of the tip sections between years 2 and 4. The more advanced erosion protection configurations (*GS* and *3Layer*) revealed greater resistance. Note that the erosion protection coating configuration *3Layer* is consumed at the tip section before year 7, whereas *GS* is able to survive the complete lifetime of

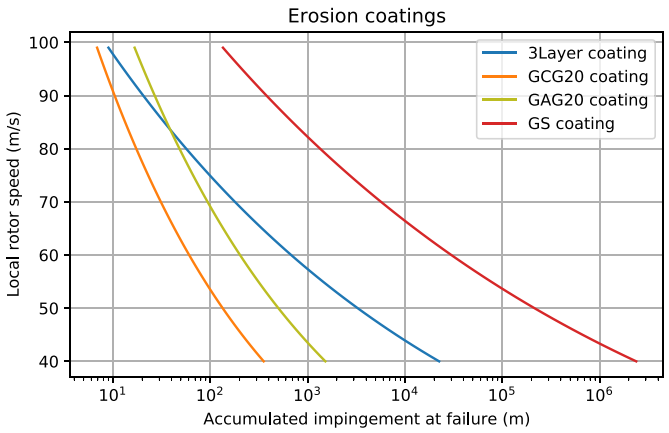

Fig. 15. Whirling arm rain erosion test data. *3Layer*: 3-layer system estimated from [14] provided by PolyTech A/S, *GC*: 1-layer elastomeric PU coating from [27]. *GA*: Generic blade coating system supplied by Olsen Wings A/S from [27]. *GS*: 3-layer system including a pink filler and PU elastomeric coating from [27]. The term *G20* (3.5 mm droplets) refers to the type of needles used for the tests.

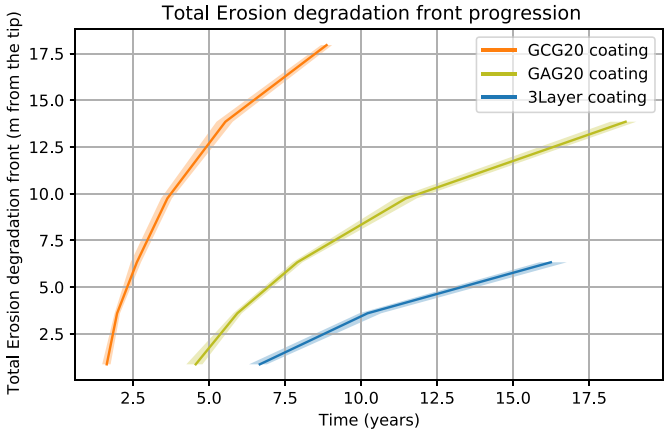

Fig. 16. Erosion front progression for the different coatings analysed (*GCG20*, *GAG20* and *3Layer*). The shadowed areas represent the 2.5–97.5% probability bands.

the turbine. With the progression of the erosion front, the laminate of the leading edge shell starts deteriorating, thus the risk of leading edge splitting increases. These results are useful for leading edge erosion maintenance planning, being able to set maintenance targets based on specific damage thresholds.

4.6. Annual energy production results

The degradation along the blade has a direct impact on the aerodynamic behaviour of the airfoils, which translates into AEP losses. The results of the analysis are shown in Fig. 17. The evolution of the AEP loss is presented into 2 phases: the incubation period and the deterioration phase. As mentioned before, during the incubation period, there are negligible effects on mass loss, aerodynamic performance, and AEP. Following the incubation period, LEP coatings start to deteriorate and the rate of increase of AEP loss is reduced throughout time in consequence of a reduction of damage with the reduction in local rotor velocity with the distance from the tip. The results reflect the complete failure of the leading edge erosion protection for sections 12 to 17 (17.5 m from the tip) using the *GC* configuration by year 9; while *GA*, *3Layer* and *GS* are not completely consumed within the service life of the wind turbine (25 years). The maximum AEP degradation for the failure of the 17.5 m of the leading edge protection for this site and turbine is between 1.5–1.75%. The *GC* configuration reaches the maximum AEP

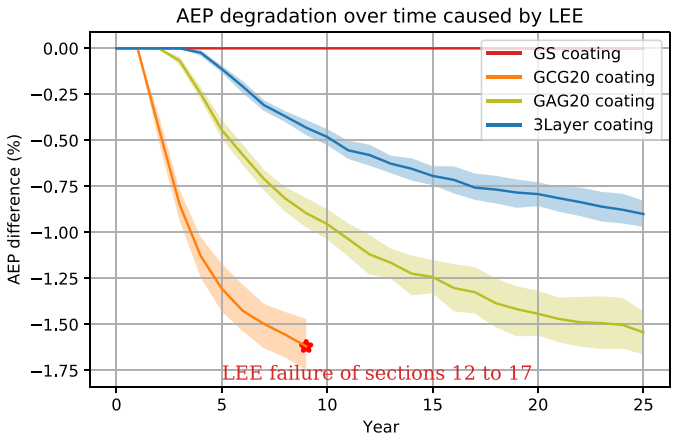

Fig. 17. AEP degradation curve for blades using the coatings analysed (*GCG20*, *GAG20* and *3Layer*). The shadowed areas represent the 2.5–97.5%. probability bands.

loss by year 9, while *GA* and *3Layer* would reach an average AEP loss of 1.5% and 0.9% at year 25 respectively. Finally, *GS* would not see its incubation period consumed, experiencing no AEP erosion-related losses in the 25 years of operation.

Notice that an important point to note is that weather-related uncertainty in the loss of AEP with respect to leading edge erosion, can be quantified whereby probabilistic scenarios can be assessed. The referred uncertainty grows with time and, for the case of study presented here, accounts for an approximate value of 0.3% AEP at the most advanced erosion stages.

5. Conclusion

An efficient leading edge erosion framework for AEP degradation erosion estimation has been presented and illustrated through a case study. The presented framework requires the aerodynamic curves of the pristine and eroded airfoils of, approximately, the outermost third of the blade (obtained through wind-tunnel tests or CFD simulations), weather (rain and wind) data of the site of study (based on on-site observations or other sources such as ERA5 reanalysis data), and erosion protection coating survivability data (based on erosion tests such as whirling arm tests). Based on this and assuming linear damage accumulation of the rain impingement model and a BEM model, the erosion and AEP degradation throughout time can be estimated. Alternatively, the aerodynamic performance of the blade can be obtained considering 3D CFD simulations. Physical testing of weathered sections of the blade can improve the accuracy of the evaluation of the aerodynamic performance of eroded airfoils.

The case study using the 5 MW NREL wind turbine located in the location of FINO1 weather station revealed the importance of designing an adequate LEP coating. For one of the LEP configurations, *GS*, the incubation period was not consumed, and no relevant AEP losses are expected. For the other configurations analysed, maximum AEP losses in the range of 0.9–1.75% have been obtained. The AEP loss for the total degradation of the blade, are in fair agreement with those reported by Eisenberg et al. [8] and Papi et al. [12]. The variability of results obtained from the use of different LEP configurations, the uncertainty of the behaviour of each sample in the rain erosion whirling arm test, and the unpredictability of the response of the LEP under local rotor velocities lower than those tested guide the requirements for the optimisation of O&M towards a model that can be dynamically updated with inspection data.

The interest of this framework relies on its capability to be applied in the development stage for O&M cost estimation, and in the operation phase for O&M planning. The variability of the erosion degradation behaviour of the sample from the whirling arm test to its actual conditions

can be overcome by updating the parameters of the power-law with inspection or SHM data through bayesian updates [47]. Qualitative damage levels, which can be identified during blade inspections, can be mapped to erosion damage intervals and used to provide an estimate of the deterioration state of the blade at different sections that would serve to better capture the particular behaviour of the erosion process of the inspected blade and plan its maintenance accordingly; degradation caused by manufacturing defects can be also be corrected in the same way. This prognosis model can provide an estimation of the current power loss of the turbine due to this phenomenon and its expected evolution, providing a tool to actively plan maintenance to avoid catastrophic failures of the blades and optimise the production of the wind turbine.

The upcoming steps of this research will be in O&M optimisation; wind turbine blade O&M will be dynamically optimised based on the prognosed evolution of the erosion corrected with inspection data. At this point, the use of different strategies including reduced tip speed operation modes, different inspection intervals, and maintenance activities considering weather constraints and the uncertainty in weather and the performance of the erosion protection coatings will be analysed.

CRediT authorship contribution statement

Javier Contreras López: Conceptualization, Methodology, Software, Writing – original draft, Writing – review & editing, Visualization. **Athanasios Kolios:** Conceptualization, Resources, Writing – review & editing, Supervision. **Lin Wang:** Conceptualization, Methodology, Validation, Writing – review & editing. **Manuel Chiachio:** Conceptualization, Writing – review & editing, Supervision, Funding acquisition.

Declaration of competing interest

The authors declare that they have no known competing financial interests or personal relationships that could have appeared to influence the work reported in this paper.

Data availability

Data will be made available on request.

Acknowledgements

This study is part of the ENHAnCE project that has received funding from the European Union's Horizon 2020 research and innovation programme under the Marie Skłodowska-Curie grant agreement No 859957. Weather data was made available by the FINO (Forschungsplattformen in Nord-und Ostsee) initiative, which was funded by the German Federal Ministry of Economic Affairs and Energy (BMWi) on the basis of a decision by the German Bundestag, organised by the Projekttraeger Juelich (PTJ) and coordinated by the German Federal Maritime and Hydrographic Agency (BSH). CFD results were obtained using the ARCHIE-WeSt High Performance Computer (www.archie-west.ac.uk) based at the University of Strathclyde.

Appendix. Acronyms

- **AEP**: annual energy production
- **AoA**: angle of attack
- **ANNs**: Artificial neural networks
- **BEM**: Blade element momentum
- **CFD**: Computational fluid mechanics
- **LEP**: Leading edge protection
- **NREL**: National Renewable Energy Laboratory
- **O&M**: Operation & Maintenance
- **SHM**: Structural Health Monitoring
- **UV**: Ultraviolet

References

[1] M.N. Scheu, L. Tremps, U. Smolka, A. Kolios, F. Brennan, A systematic failure mode effects and criticality analysis for offshore wind turbine systems towards integrated condition based maintenance strategies, Ocean Eng. 176 (2019) 118–133.
[2] N. Gaudern, A practical study of the aerodynamic impact of wind turbine blade leading edge erosion, in: Journal of Physics: Conference Series, Vol. 524, IOP Publishing, 2014, 012031.
[3] J. Contreras, A. Kolios, Risk-based maintenance strategy selection for wind turbine composite blades, Energy Rep. (2022) (on–line).
[4] H. Slot, E. Gelinck, C. Rentrop, E. Van Der Heide, Leading edge erosion of coated wind turbine blades: Review of coating life models, Renew. Energy 80 (2015) 837–848.
[5] L. Mishnaevsky Jr., C.B. Hasager, C. Bak, A.-M. Tilg, J.I. Bech, S.D. Rad, S. Fæster, Leading edge erosion of wind turbine blades: Understanding, prevention and protection, Renew. Energy 169 (2021) 953–969.
[6] A. Sareen, C.A. Sapre, M.S. Selig, Effects of leading edge erosion on wind turbine blade performance, Wind Energy 17 (10) (2014) 1531–1542.
[7] M. Schramm, H. Rahimi, B. Stoevesandt, K. Tangager, The influence of eroded blades on wind turbine performance using numerical simulations, Energies 10 (9) (2017) 1420.
[8] D. Eisenberg, S. Laustsen, J. Stege, Wind turbine blade coating leading edge rain erosion model: Development and validation, Wind Energy 21 (10) (2018) 942–951.
[9] G.S. Springer, Erosion by Liquid Impact, Osti, 1976.
[10] A. Shourangiz-Haghighi, M.A. Haghnegahdar, L. Wang, M. Mussetta, A. Kolios, M. Lander, State of the art in the optimisation of wind turbine performance using CFD, Arch. Comput. Methods Eng. 27 (2) (2020) 413–431.
[11] L. Cappugi, A. Castorrini, A. Bonfiglioli, E. Minisci, M.S. Campobasso, Machine learning-enabled prediction of wind turbine energy yield losses due to general blade leading edge erosion, Energy Convers. Manage. 245 (2021) 114567.
[12] F. Papi, F. Balduzzi, G. Ferrara, A. Bianchini, Uncertainty quantification on the effects of rain-induced erosion on annual energy production and performance of a multi-mw wind turbine, Renew. Energy 165 (2021) 701–715.
[13] C. Hasager, F. Vejen, J. Bech, W. Skrzypiński, A.-M. Tilg, M. Nielsen, Assessment of the rain and wind climate with focus on wind turbine blade leading edge erosion rate and expected lifetime in danish seas, Renew. Energy 149 (2020) 91–102.
[14] J.I. Bech, C.B. Hasager, C. Bak, Extending the life of wind turbine blade leading edges by reducing the tip speed during extreme precipitation events, Wind Energy Sci. 3 (2) (2018) 729–748.
[15] C.B. Hasager, F. Vejen, W.R. Skrzypiński, A.-M. Tilg, Rain erosion load and its effect on leading-edge lifetime and potential of erosion-safe mode at wind turbines in the north sea and baltic sea, Energies 14 (7) (2021) 1959.
[16] M.H. Keegan, D. Nash, M. Stack, On erosion issues associated with the leading edge of wind turbine blades, J. Phys. D: Appl. Phys. 46 (38) (2013) 383001.
[17] R. Herring, K. Dyer, F. Martin, C. Ward, The increasing importance of leading edge erosion and a review of existing protection solutions, Renew. Sustain. Energy Rev. 115 (2019) 109382.
[18] W. Han, J. Kim, B. Kim, Effects of contamination and erosion at the leading edge of blade tip airfoils on the annual energy production of wind turbines, Renew. Energy 115 (2018) 817–823.
[19] H. Law, V. Koutsos, Leading edge erosion of wind turbines: Effect of solid airborne particles and rain on operational wind farms, Wind Energy 23 (10) (2020) 1955–1965.
[20] A. Castorrini, A. Corsini, F. Rispoli, P. Venturini, K. Takizawa, T.E. Tezduyar, Computational analysis of performance deterioration of a wind turbine blade strip subjected to environmental erosion, Comput. Mech. 64 (4) (2019) 1133–1153.
[21] G. Fiore, M.S. Selig, Simulation of damage for wind turbine blades due to airborne particles, Wind Eng. 39 (4) (2015) 399–418.
[22] H. Slot, E. Gelinck, C. Rentrop, E. van der Heide, Leading edge erosion of coated wind turbine blades: Review of coating life models, Renew. Energy 80 (2015) 837–848.
[23] 3M, A 3 M Study is the First to Show the Effects of Erosion on Wind Turbine Efficiency, Tech. rep., 3M, 2011.
[24] L. Mishnaevsky, K. Branner, H.N. Petersen, J. Beauson, M. McGugan, B.F. Sørensen, Materials for wind turbine blades: an overview, Materials 10 (11) (2017) 1285.
[25] L. Mishnaevsky Jr., Toolbox for optimizing anti-erosion protective coatings of wind turbine blades: overview of mechanisms and technical solutions, Wind Energy 22 (11) (2019) 1636–1653.
[26] E. Cortés, F. Sánchez, A. O'Carroll, B. Madramany, M. Hardiman, T.M. Young, On the material characterisation of wind turbine blade coatings: the effect of interphase coating–laminate adhesion on rain erosion performance, Materials 10 (10) (2017) 1146.
[27] N. Johansen, Test Methods for Evaluating Rain Erosion Performance of Wind Turbine Blade Leading Edge Protection Systems (Ph.D. thesis), Technical University of Denmark, 2020.

[28] Instruction: Blade inspections, 2016.
[29] K. Latoufis, V. Riziotis, S. Voutsinas, N. Hatziargyriou, Effects of leading edge erosion on the power performance and acoustic noise emissions of locally manufactured small wind turbine blades, in: Journal of Physics: Conference Series, Vol. 1222, IOP Publishing, 2019, 012010.
[30] M. Elhadi Ibrahim, M. Medraj, Water droplet erosion of wind turbine blades: Mechanics, testing, modeling and future perspectives, Materials 13 (1) (2020) 157.
[31] S. Zhang, K. Dam-Johansen, S. Nørkjær, P.L. Bernad Jr., S. Kiil, Erosion of wind turbine blade coatings–design and analysis of jet-based laboratory equipment for performance evaluation, Prog. Org. Coat. 78 (2015) 103–115.
[32] ASTM, Standard Test Method for Liquid Impingement Erosion using Rotating Apparatus, Standard, ASTM, 2021.
[33] J.I. Bech, N.F.-J. Johansen, M.B. Madsen, Á. Hannesdóttir, C.B. Hasager, Experimental study on the effect of drop size in rain erosion test and on lifetime prediction of wind turbine blades, Renew. Energy 197 (2022) 776–789.
[34] A.S. Verma, Z. Jiang, M. Caboni, H. Verhoef, H. van der Mijle Meijer, S.G. Castro, J.J. Teuwen, A probabilistic rainfall model to estimate the leading-edge lifetime of wind turbine blade coating system, Renew. Energy 178 (2021) 1435–1455.
[35] J. Chen, J. Wang, A. Ni, A review on rain erosion protection of wind turbine blades, J. Coat. Technol. Res. 16 (1) (2019) 15–24.
[36] H. Hersbach, B. Bell, P. Berrisford, S. Hirahara, A. Horányi, J. Muñoz-Sabater, J. Nicolas, C. Peubey, R. Radu, D. Schepers, et al., The era5 global reanalysis, Q. J. R. Meteorol. Soc. 146 (730) (2020) 1999–2049.
[37] J.R. Norris, J.R. Norris, Markov Chains, no. 2 in 1, Cambridge University Press, 1998.
[38] Forschungs- und Entwicklungszentrum Fachhochschule Kiel GmbH, Forschungsplattformen in nordund ostsee nr. 1, 2, 3, 2022, data retrieved from FINO1 Database, https://www.fino-offshore.de/de/index.html.
[39] F. Menter, Zonal two equation kw turbulence models for aerodynamic flows, in: 23rd Fluid Dynamics, Plasmadynamics, and Lasers Conference, 1993, p. 2906.
[40] A.K. Ravishankara, H. Özdemir, E. van der Weide, Analysis of leading edge erosion effects on turbulent flow over airfoils, Renew. Energy 172 (2021) 765–779.
[41] L.A. Viterna, R.D. Corrigan, Fixed Pitch Rotor Performance of Large Horizontal Axis Wind Turbines, NASA, 1982.
[42] OpenFAST, 2017, https://github.com/OpenFAST/openfast, accessed: 2021-12-20.
[43] A. Best, The size distribution of raindrops, Q. J. R. Meteorol. Soc. 76 (327) (1950) 16–36.
[44] L. Ziegler, N. Cosack, A. Kolios, M. Muskulus, Structural monitoring for lifetime extension of offshore wind monopiles: Verification of strain-based load extrapolation algorithm, Mar. Struct. 66 (2019) 154–163.
[45] J. Jonkman, S. Butterfield, W. Musial, G. Scott, Definition of a 5-mw Reference Wind Turbine for Offshore System Development, Tech. rep., National Renewable Energy Lab.(NREL), Golden, CO (United States), 2009.
[46] W. Timmer, An overview of naca 6-digit airfoil series characteristics with reference to airfoils for large wind turbine blades, in: 47th AIAA Aerospace Sciences Meeting Including the New Horizons Forum and Aerospace Exposition, 2009, p. 268.
[47] J. Chiachío, M.L. Jalon, M. Chiachío, A. Kolios, A markov chains prognostics framework for complex degradation processes, Reliab. Eng. Syst. Saf. 195 (2020) 106621.